# Exploring Charge Migration in Light-Harvesting Complexes Using Electron Paramagnetic Resonance Line Narrowing

**Nagarajan Srivatsan**[†]

*Division of Chemistry and Chemical Engineering, Mail Stop 127-72, California Institute of Technology, Pasadena, California 91125*

**Stefan Weber**[‡]

*Institute of Experimental Physics, Free University Berlin, Arnimallee 14, 14195 Berlin, Germany*

**Dmitri Kolbasov**[§]

*Department of Chemistry, University of Chicago, 5735 South Ellis Avenue, Chicago, Illinois 60637*

**James R. Norris***

*Department of Chemistry and Institute of Biodynamics, University of Chicago, 5735 South Ellis Avenue, Chicago, Illinois 60637*

*Received: January 24, 2002; In Final Form: June 19, 2002*

The light-harvesting protein complex 1 (LH1) of the purple bacterium *Rhodobacter sphaeroides* exhibits EPR signals upon treatment with oxidizing reagents such as potassium ferricyanide. These signals are assigned to radical cations of the LH1's bacteriochlorophyll pigments, B880•$^+$. An intriguing feature of the B880•$^+$ EPR spectrum is the narrow line width exhibited relative to in vitro monomeric BChl*a*•$^+$ and the primary donor radical cation of the photosynthetic reaction center's "special pair", P•$^+$. In this paper, we investigate the temperature and oxidant concentration dependence of the B880•$^+$ EPR spectrum with the aim of elucidating the mechanism for spectral line narrowing. The experimental data are interpreted in terms of EPR line narrowing that accompanies charge migration and spin exchange. For charge migration, the line-narrowing models are driven by standard, nonadiabatic electron transfer assisted by vibronic coupling. The results are consistent with a hypothesis that, in LH1, the EPR spectral shape is dominated by electron transfer instead of spin exchange. In addition, the electronic and energetic factors governing the inter-BChl*a* cryogenic charge transport are explored. Using standard treatments, large reorganization energy and weak electronic coupling are obtained for the charge migration process. The EPR results support the view that highly delocalized radical cation states similar to that observed for the primary donor BChl*a*s of the special pair of the photosynthetic reaction center do not occur in oxidized LH1 complexes in the 6−300 K temperature range. However, the EPR results are compatible with a highly asymmetrical version of the special pair. The unrealistically high value of reorganization energy for electron transfer is attributed to treating the charge migration process as if electron transfer were homogeneous. A more realistic value of reorganization energy is predicted to result if free-energy heterogeneity were to be included in modeling electron transfer in LH1.

## I. Introduction

The initial energy conversion steps of photosynthesis involve two types of pigment−protein assemblies, the antenna complexes and the reaction centers (RCs). The antenna complexes absorb light and efficiently transport the excitation energy to the RCs, where the energy is utilized to initiate electron-transfer reactions.[1] In purple bacteria, the energy absorption and transportation processes are generally mediated by two structurally similar antenna complexes, LH1 and LH2. X-ray crystal structures for LH2 complexes and RCs from a few purple bacterial species have been elucidated.[2−6] Additionally, an electron density projection map at a resolution of 0.85 nm has been determined for LH1.[7] These structures form the basis for understanding the electronic characteristics and the function of the bacterial photosynthetic unit.

The constituent bacteriochlorophyll *a* (BChl*a*) pigments of LH1 complexes exhibit red-shifted absorption spectra relative to the in vitro monomeric species. The monomer $Q_y$ transition generally occurs at about 773 nm, whereas in LH1 this transition is shifted to approximately 880 nm. Similar red-shifted absorption characteristics are also exhibited by the BChl*a*s in LH2 and the RC primary electron donor. The bathochromic shifts occur mainly due to excitonic and exchange type interactions, which are fostered by the close proximities of the pigments in the photosynthetic proteins.[8−20] For instance, the "special pair"

* Corresponding author. Phone: +1 (773) 702 7864. FAX: (773) 702 9646. E-mail: j-norris@uchicago.edu.
† Phone: +1 (626) 395 3964. E-mail: vatsan@caltech.edu.
‡ Phone: +49 (30) 838 56139. FAX: +49 (30) 838 56046. E-mail: Stefan.Weber@physik.fu-berlin.de.
§ Phone: +1 (773) 702 9646. FAX: +1 (773) 702 0805. E-mail: dkolbaso@uchicago.edu.

10.1021/jp0255233 CCC: $25.00 
Published on Web 02/11/2003

of BChl*a*s (P865) of the RC primary donor exhibit face-to-face separations of only about 0.4 nm. In principle, the basic unit of LH2 could be an analogous BChl*a* dimer (B850), which is held between a pair of membrane spanning peptides, $\alpha$ and $\beta$. The $\beta$-peptide binds an additional BChl*a* (B800) that is located about 1.7 nm below the B850s. In functional proteins, which are $C_n$ symmetric ($n = 8$ or 9), the B850s form an overlapping circular array, whereas the B800s form a complex with well-separated pigments. Some LH1 complexes are rotationally symmetric oligomers of $\alpha\beta$-units such as LH2, with the exception that the B800s are absent. The 0.85-nm resolution projection map determined for LH1 shows a ring composed of 16 $\alpha\beta$-units. Studies of LH1−RC core complexes have indicated that the $\alpha\beta$-units of LH1 and their corresponding BChl*a*s (B880s) form a circular array similar to the B850 ring around the RC.[21−27] One exception appears to be membranes of *Rhodobacter* (*Rb.*) *sphaeroides* deficient in LH2 complexes.[28] The close proximities of the BChl*a*s in the B850 and B880 rings engender significant electronic couplings, which in turn facilitate efficient, ultrafast energy transport within these arrays. Such interactions additionally produce delocalized excited states in the B850, B880, and P865 clusters of the antenna complexes and RCs.[29]

In the case of P865, the electronic interactions between the BChl*a*s also result in delocalized ground states. This was first deduced from EPR measurements on P865$\bullet^+$. At X-band frequencies (9−10 GHz), P865$\bullet^+$ exhibits a Gaussian line shape with a relatively temperature independent width of about 0.95 mT. The width, which is reduced compared to the 1.35 mT width detected for monomeric BChl*a*$\bullet^+$, and the shape are due to asymmetric (approximately 2 to 1) delocalization of the spin over two BChl*a*s.[30−32] In the case of LH1, room temperature X-band EPR spectra have been reported for oxidized complexes from several species.[33−36] The line shapes were reported to be approximately Gaussian with widths of about 0.4 mT. These signals were assigned to radical cations of the BChl*a*s that comprise the LH1 B880 ring. The observed line narrowing was attributed to either delocalization or rapid electron transfer over the B880 ring. In this context, "rapid" means so fast that further acceleration would not cause any additional decrease in the observed line width. This limiting value of the line width is inversely proportional to $\sqrt{N}$, where $N$ is the number of BChl*a*s. This interpretation suggests that the LH1 BChl*a*s are strongly coupled in the ground state, similar to P865. In the aforementioned B880$\bullet^+$ studies, however, other line narrowing mechanisms such as (slower) thermally activated electron transfer and spin exchange were not considered and experimentally addressed. The question of whether the unpaired electron spin in B880$\bullet^+$ is delocalized or whether spin migration occurs due to dynamical processes is of interest since this has implications for the description of the electronic structure of the B880 ring. The aim of this study is to elucidate the B880$\bullet^+$ EPR line narrowing mechanism and thereby gain some insight into the strength of the inter-BChl*a* ground-state interactions.

We have investigated the oxidant concentration and temperature dependence of the B880$\bullet^+$ EPR spectral characteristics at X-band. The B880$\bullet^+$ species was elicited by oxidation of LH1 with potassium ferricyanide (PF) similar to the procedure used in previous studies.[33−36] Data were acquired for oxidized detergent-isolated LH1 complexes from *Rb. sphaeroides* strain *puc*705-BA, which is a mutant deficient in LH2 complexes. Measurements were also conducted on oxidized membrane-bound LH1 complexes from *Rb. sphaeroides* strain M2192, which is a mutant deficient in LH2 and RCs.

## II. Experimental Section

**A. Preparation of LH1 Complexes.** Frozen cells of *Rb. sphaeroides puc*705-BA were thawed and suspended in Tris buffer (a solution of 10 mM tris(hydroxymethyl)aminomethane hydrochloride and 0.01 mM ethylenediamminetetraacetic acid disodium salt in distilled water at pH 7.8.) containing 100 mM NaCl. The suspension was passed through a prechilled French press at 16 000 psi in order to rupture the cells. The debris was sedimented by low-speed centrifugation at 12 000 rpm and then removed. The supernatant was centrifuged at 45 000 rpm for 180 min, and this yielded the photosynthetic membranes as the sediment. The membranes were suspended in Tris buffer such that the 1 cm path length absorbance at 850 nm was about 50, and then they were solubilized by the addition of 1-*O*-octyl-$\beta$-D-glucopyranoside (BOG) to a final concentration of 2% (w/v). The protein solubilization was accomplished by stirring the suspension at ambient temperature for about 1 h. The solubilized material was centrifuged at 45 000 rpm for 180 min in order to sediment the leached membranes. Crude preparations of the photosynthetic complexes were obtained by subjecting the supernatant to fractional precipitation using ammonium sulfate as the precipitant. As verified by EPR spectroscopy, the RCs with the characteristic intense photoinduced EPR signal of peak-to-peak line width of approximately 0.96 mT precipitated while LH1 complexes with no photoinduced EPR signal remained in solution. The RCs had their characteristic optical maximum at 880 nm. As further verification of the LH1 preparation, the LH1 complexes exhibited an optical maximum at 880 nm and a provided narrower EPR signal of line width 0.4 (at $T = 23$ °C) upon chemical oxidation by potassium ferricyanide in the dark. An EPR line width of 0.38−0.41 mT was observed in chromatophores of a photoreaction centerless mutant, *Rhodospirillum* (*Rs.*) *rubrum* strain F24, and was assigned to the antenna complex.[35] Before separation into a RC precipitation and LH1 solution, the intact preparation gave a composite EPR signal clearly showing the 0.96 mT wide RC signal superimposed on the narrower LH1 signal. Light irradiation induced only the broad 0.96 mT signal of the RC. Both signals, i.e., the narrow 0.4 mT signal and the broader 0.96 signal, could be produced by chemical oxidation in the dark, with the initial stage of the oxidation only creating the broader, RC-EPR signal.

The LH1 proteins were dissolved in a minimal amount of Tris buffer containing 0.8% (w/v) BOG and dialyzed overnight against the same buffered detergent solution. The LH1 complexes were further purified by column chromatography. In a typical procedure, the protein was loaded onto a DEAE-cellulose column that was preequilibrated with BOG, washed with a 0.1 M NaCl solution in BOG, and then eluted by increasing the NaCl concentration in BOG to 0.28 M. This overall procedure is similar to previous preparations.[17,35,37] Finally, on the basis of a low-resolution 8.5 Å projection map of similarly detergent-isolated LH1, a circular aggregate with 16-fold symmetry with 32 bacteriochlorophyll molecules has been proposed.[7] Although 16-fold symmetry may suggest monodispersed aggregates of LH1, the minimum requirement for this EPR study is that few LH1 aggregates have sizes that contain less than about 16 BChls, i.e., large enough that spin transfer can sample a sufficient number of molecules to account for the EPR line narrowing.

**B. Generation of Radical Cations.** Radical cations of the LH1 complexes were generated by oxidation with potassium ferricyanide (PF) under ambient conditions. Stock solutions of PF were prepared in Tris buffer and used immediately. The concentrations were in the 1 mM to 1 M range. The protein oxidations were accomplished via the following procedure. A

few microliters of the PF solution were added to 300 $\mu$L of the protein sample contained in an Eppendorf tube. Following this, the detergent isolated proteins were vortexed for 5 s. In the case of membrane-bound complexes, it was necessary to sonicate the samples for about 30 s to generate the radical cations. The UV/visible spectra of the oxidized proteins were measured, and the samples were then transferred to glass EPR tubes and frozen in liquid nitrogen. The entire procedure from the time of addition of the PF solution until freezing typically took about 4 min.

The 1 mm path length absorbencies of the proteins prior to oxidation were as follows. For detergent-isolated LH1, $A_{882} = 2.061$; and for membrane bound LH1, $A_{878} = 1.822$. Radical cations of detergent-isolated LH1 were generated with 7 $\mu$M to 40 mM final concentrations of PF. Sonication and larger oxidant concentrations (8−143 mM final concentrations of PF) were required to elicit similar NIR absorbance changes and EPR signals from the membrane-bound samples, most likely because the membrane lipids form an effective barrier to PF.

**C. UV/Visible Measurements.** Spectra for the LH1 complexes were measured under ambient conditions with a Shimadzu UV-1601 spectrophotometer. Quartz cuvettes of 1 mm path length were used for all measurements. The fraction ($\chi$; $\chi = \Delta A/A$) of the LH1 near-infrared (near-IR) band bleached by the PF treatment was calculated from spectra measured before and after oxidation of the complexes. The absorbencies were corrected for decreases due to dilution prior to calculating $\chi$. The spectra acquired for detergent-isolated proteins showed flat baselines with essentially zero offsets. Therefore, $\chi$ could be calculated from the near-IR absorbance maxima of the spectra measured before and after oxidation. The membrane-bound LH1 complexes, however, exhibited spectra with nonzero baselines due to scattering by the membrane particles. In addition, spectra measured before and after the oxidation procedure displayed nonidentical baselines. This is probably because the sonication step produced a different distribution of vesicle sizes. The $\chi$ values for the membrane-bound LH1 samples were obtained via the following procedure. The spectra were first digitally fit with a function that consisted of a sum of Gaussians and a linear baseline term. The baseline terms were then subtracted from the measured spectra. The near-IR absorbance maxima were determined from the baseline corrected spectra, and these were used to calculate $\chi$.

**D. EPR Measurements.** Spectra were acquired with Varian Century Line Series E-112 spectrometers equipped with liquid nitrogen Dewar inserts. The sample temperatures were measured with calibrated copper−constantan or gold−chromel thermocouples. In either case, the thermocouple was embedded in the sample. Spectra were also measured with a laboratory built spectrometer, which consisted of a Bruker ER041 microwave bridge and a Varian E-9 magnet. The resonator used was either a Bruker ER 4118100 split-ring resonator (for experiments below 100 K) or a Bruker ER 4118X-MD-5W1 dielectric resonator (for experiments at $T \geq 100$ K). These were immersed in a helium flow cryostat. The sample temperatures were measured with a silicon diode sensor that was placed in proximity to the resonator and set with a Lakeshore 321 temperature controller. The operating frequencies of the spectrometers were between 9 and 10 GHz. A modulation frequency of 100 kHz was used for all measurements. Spectrometer parameters such as the microwave power, modulation amplitude, time constant, and scan rate were chosen to obtain undistorted spectra.

EPR line shape parameters were extracted by digitally fitting the spectra with either a Voigt profile, which is a Gaussian convolved with a Lorentzian, or a sum of Gaussians. In the latter function, the positions of the Gaussians were set to be identical to one another. A linear term was added to both functions in order to describe the experimental baseline. The data fitting programs employed a nonlinear least squares routine based on the Levenberg−Marquardt algorithm. The Voigt profile program was implemented according to the procedure of Smirnov and co-workers[38] When the Voigt profile was used to fit the data, the envelope line width ($\Delta H_T$) was calculated directly from the Gaussian ($\Delta H_G$) and Lorentzian ($\Delta H_L$) widths as $\Delta H_T = 0.5[\Delta H_L + (\Delta H_L^2 + 4\Delta H_G^2)^{1/2}]$. When the sum of Gaussians was employed, $\Delta H_T$ was extracted by means of the following procedure. First, the best fit to the spectrum was obtained. Then the extrema of the fit function and the corresponding magnetic field loci were determined via a one-dimensional minimization procedure. Finally, the line width was obtained as the difference between the magnetic field loci of the extrema.

## III. Results and Discussion

The 0.4 mT room temperature EPR line width of B880$\bullet^+$ is significantly reduced relative to that measured for monomeric BChl*a*$\bullet^+$, which in solvents such as dichloromethane and methanol exhibits an approximately temperature independent Gaussian spectrum with the line width of 1.3−1.35 mT.[39] The line shape characteristics are due to unresolved hyperfine interactions that produce inhomogeneous broadening of the spectrum. The width of the B880$\bullet^+$ spectrum is reduced either by delocalization or by dynamical processes such as electron transfers and spin exchange. The reason for such narrowing is that each spin experiences an averaged hyperfine influence from several monomers such that the statistical average always has a narrower distribution than the hyperfine distribution of a monomer BChl*a*$\bullet^+$. Different line-narrowing mechanisms generally result in different spectral shapes. In the case of orbital delocalization, i.e., when the electronic orbitals are linear combinations of the monomer molecular orbitals, inhomogeneously broadened Gaussian line shapes with temperature-independent spectral characteristics are expected.[30,31,39,40] For narrowing due to spin exchange and electron transfer, the spectral characteristics depend on the dimensionality and rate of the process.[41] The spectral lines are generally non-Gaussian, but tend to the Gaussian form when the rate of the process is either very low or very high. Delocalization and dynamic line narrowing mechanisms can operate concurrently. That is, electron transfer and/or spin exchange may proceed between some number of basic electron spin units. This basic element consists of a few BChl*a*s over which the unpaired electron is delocalized. We note that ordinary continuous wave EPR spectroscopy cannot distinguish a very fast electron transfer from a true delocalization.

**A. Variation of the B880$\bullet^+$ Spectral Parameters with Oxidant Concentration.** The UV/visible and EPR spectra for this study were measured at ambient temperatures and $T = 205.6$ K, respectively. The low temperature was selected to obtain reasonable signal strengths from the mildly oxidized LH1 samples. Parts A and B of Figure 1 display the near-IR regions of absorption spectra measured for detergent-isolated and membrane-bound LH1 that were reacted with PF. The decreased absorbance at about 880 nm is due to the oxidation of the LH1's BChl*a* chromophores. The bleach is enhanced with increasing PF concentration, indicating that a larger fraction of the B880 molecules is oxidized. The extent of oxidation is quantified by $\chi = \Delta A/A$, which is to a good approximation proportional to

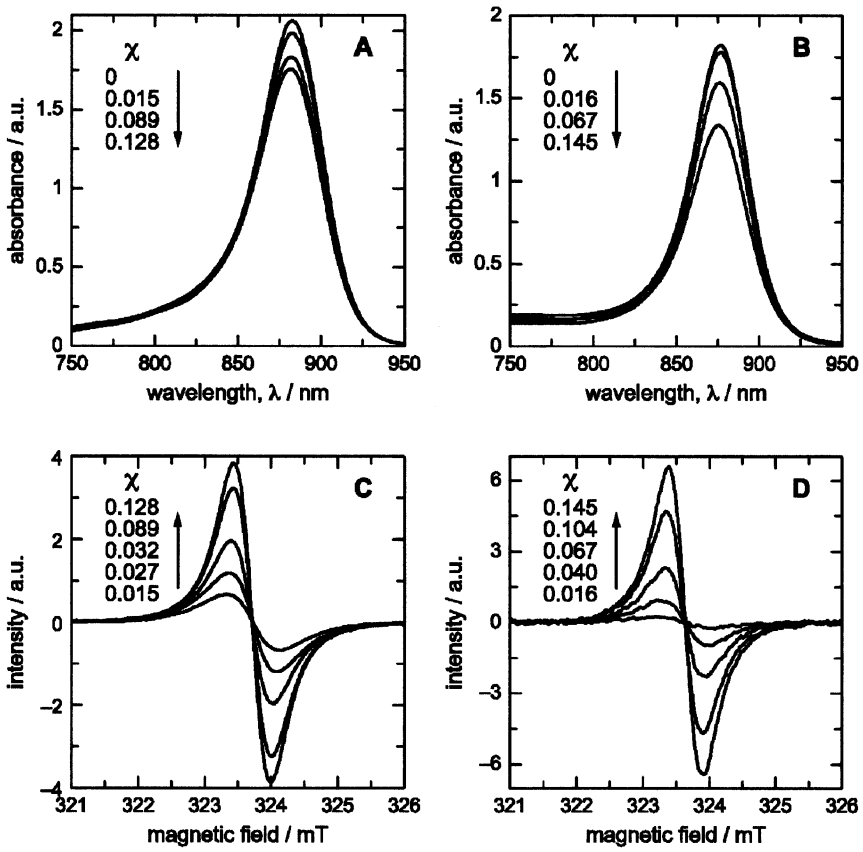


**Figure 1.** (Top panels) Near-IR regions of absorption spectra measured at $T = 298$ K for (A) detergent-isolated and (B) membrane-bound LH1 complexes oxidized with PF. The fraction $\chi = \Delta A/A$ of the near-IR band bleached by the PF treatment was calculated from the absorbance maxima of spectra that were corrected for dilution. (Bottom panels) EPR spectra measured at $T = 205.6$ K for (C) detergent-isolated and (D) membrane-bound B880$^{\bullet+}$ species that were elicited by the chemical oxidation of LH1 complexes. The signal amplitudes are enhanced with a decrease of the near-IR absorbance, which demonstrates that the spectra are due to oxidized LH1 BChl*a*s.

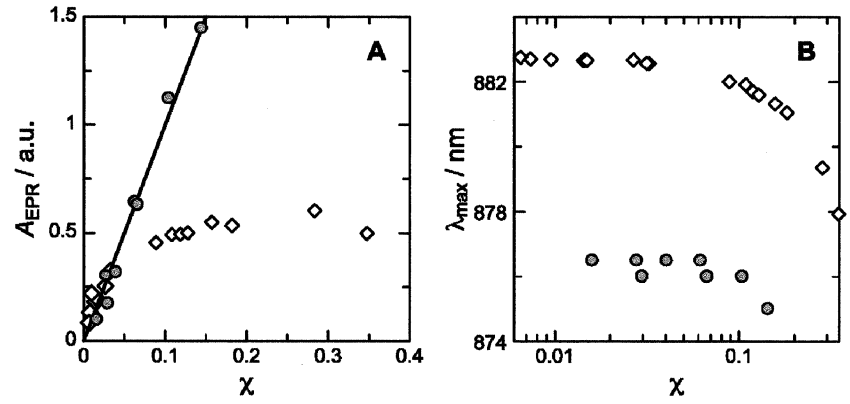


**Figure 2.** (A) Variation of the EPR spectral area ($A_{EPR}$) with the fraction ($\chi$) of the LH1 near-IR absorbance bleached by oxidation for (open diamonds) detergent-isolated and (filled circles) membrane-bound complexes. (B) Dependence of the wavelength position ($\lambda_{max}$) of the near-IR absorbance maxima on $\chi$ for (open diamonds) detergent-isolated and (filled circles) membrane-bound complexes.

the concentration of the oxidized BChl*a* species. The PF concentrations used in this study yielded $\chi$ in the range of 0.002−0.35 for detergent-isolated LH1 and values ranging from 0.016 to 0.145 for the membrane-bound complexes. Parts C and D of Figure 1 show EPR spectra that were acquired for oxidized LH1 samples. Increasing the fraction of oxidized pigments, $\chi$, results in enhanced signal amplitudes that demonstrate the EPR results from oxidized BChl*a*s in LH1.

*A.1. Stability of B880*$^{\bullet+}$. The correlation of the B880$^{\bullet+}$ EPR (integrated) spectral area ($A_{EPR}$) to the fraction of oxidized B880 molecules provides information regarding the stability of the B880$^{\bullet+}$ species. Ideally, a stable B880$^{\bullet+}$ species would constitute the sole product of LH1 oxidation. If this were correct, then $\chi$ would be proportional to the concentration of generated radical cations, as is $A_{EPR}$. The two quantities are thus expected to be linearly related, provided quantitative conversion of B880 to stable B880$^{\bullet+}$ is achieved. Figure 2A displays graphs of $A_{EPR}$ versus $\chi$. For detergent-isolated LH1, $A_{EPR}$ exhibits a linear dependence on $\chi$ for values up to about 0.05, beyond which significant deviation from linearity is observed. In conjunction with the observation that only B880$^{\bullet+}$ EPR signals are detected, the results suggest that at $\chi > 0.05$, the B880$^{\bullet+}$ species degrade to form diamagnetic products. For membrane-bound complexes, a linear variation is discerned in the entire investigated range. The linear variation of $A_{EPR}$ up to 5% NIR bleach for detergent-isolated proteins and up to 15% for membrane-bound complexes

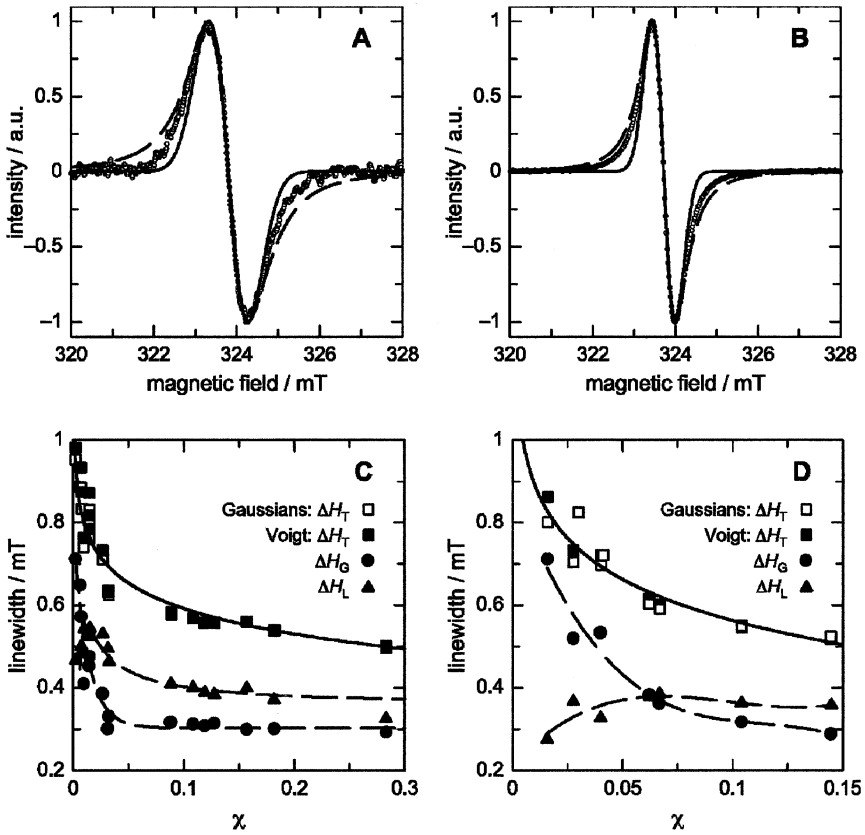


**Figure 3.** (Top panels) B880•$^+$ EPR spectra measured at $T = 205.6$ K for oxidized detergent-isolated LH1 samples that exhibited (A) 0.2% ($\chi = 0.002$) and (B) 12.8% ($\chi = 0.128$) bleach of the near-IR absorbencies. The solid and dashed lines represent Gaussian and Lorentzian curves calculated with the widths of the experimental spectra, $\Delta H_T = 0.95$ mT (A) and $\Delta H_T = 0.56$ mT (B). (Bottom panel) Variation of (C) detergent-isolated and (D) membrane-bound B880•$^+$ EPR line shape parameters with the fraction $\chi$ of the LH1 near-IR absorbance bleached by oxidation. The parameter $\Delta H_T$ denotes the envelope peak-to-peak line width determined by fitting the spectra with either a sum of Gaussians or the Voigt profile, and $\Delta H_G$ and $\Delta H_L$ denote the widths of the Gaussian and Lorentzian components of the Voigt profile.

delineate the regimes where B880•$^+$ EPR measurements yield information for LH1 with the full complement of B880s.

The integrity of B880•$^+$ can also be judged from the changes of the near-IR characteristics and from the reversibility of the oxidation process. Studies in this regard have involved oxidation of LH1 with PF followed by treatment of the oxidation product with sodium ascorbate or sodium dithionite. Picorel and co-workers reported that the redox reactions of LH1 are extremely rapid and that nearly all of the near-IR bleach caused by oxidation can be recovered by the addition of excess sodium ascorbate.[36] These results were obtained for detergent-isolated LH1 complexes from *Rhodospirillum rubrum*, *Rb. Sphaeroides*, and *Ectothiorhodospira sp*. The oxidations were affected with concentrations of PF in the 1−300 mM range. Regardless, our linear relationship between EPR spins and optical bleaching establishes that the EPR signal arises from one-electron oxidized BChl. In addition, in our linear region, reduction of the cation in membrane bound LH1 complexes by ascorbate returns at least 90% of the unoxidized optical spectrum, again supporting the view that the chemistry is mostly reversible in the concentration ranges that apply to these EPR studies.

Law and co-workers have investigated the redox properties of detergent-isolated LH1 complexes from *Rhodobium marinum*.[42] The proteins were first treated with PF in the 1−100 mM range and then reacted with an excess of either sodium ascorbate or sodium dithionite. The LH1 NIR bleach was not recovered, which indicates an irreversible oxidation process. It was additionally reported that $\lambda_{max}$ exhibited a considerable blue shift with time. This probably occurs due to the loss of inter-BChl*a* interactions caused either by the oxidation of the B880s or by the destruction of the protein structure. However, the shifting of $\lambda_{max}$ does not necessarily require the destruction of the B880s or LH1. This is because if sufficient concentrations of B880•$^+$ are generated, then the concomitant loss of excitonic interactions would also engender a blue-shifted band. In our studies, the stability of detergent isolated LH1 complexes is less than that of membrane bound LH1, in agreement with the work of Law and co-workers[42] and Picorel and co-workers.[36] With regard to reversibility or lack of reversibility, the key to our EPR study is the one-to-one correspondence between cation radical production and BChl bleaching as indicated by the linear relationship between optical bleaching and EPR area, which we take as strong evidence for the production of BChl$^+$.

In this study, a blue shift of the NIR absorption band was detected for the more severely oxidized LH1 samples. Figure 2B displays a graph of $\lambda_{max}$ versus $\chi$. Little or no variation is detected for $\chi \leq 0.05$, beyond which a systematic blue shift is observed. These results corroborate the conclusions drawn from the $A_{EPR}$ versus $\chi$ study. We note that for detergent-isolated LH1 complexes the linear $A_{EPR}$ and flat $\lambda_{max}$ versus $\chi$ regimes correspond to samples oxidized with PF concentrations in the 7−100 $\mu$M range, as compared to the 1−300 mM concentrations used in the previous studies.

*A.2. Spin Exchange in the B880 Complex.* Parts A and B of Figure 3 display EPR spectra of detergent-isolated LH1 samples that were oxidized to different extents. These are compared to Gaussian and Lorentzian curves calculated with the peak-to-peak widths of the experimental spectra. The B880•$^+$ line shapes are intermediate to the calculated curves. This was found to be the case at all of the investigated $\chi$ values. It was additionally

observed that the line widths progressively decreased with increasing $\chi$. Similar variations of line shapes and widths were also detected for membrane-bound samples.

The experimental spectra were fit with the Voigt profile to better characterize the trend of the line shapes and widths. Parts C and D of Figure 3 display the $\chi$ dependence of the total peak-to-peak line width ($\Delta H_T$) versus the Gaussian ($\Delta H_G$) and Lorentzian ($\Delta H_L$) components of the width for detergent-isolated and membrane-bound LH1. The figures additionally display a value for the total line width, $\Delta H_T$, that was determined by fitting the spectra with a sum of Gaussians. The total line widths extracted from the different fit functions were typically identical within a few percent. Clearly, the B880•$^+$ EPR line widths are extremely sensitive to the concentration of generated radical cations. The line width exhibits an initial rapid decrease followed by a slower decrease as $\chi$ increases. The line shape descriptors, $\Delta H_G$ and $\Delta H_L$, also exhibit variations. The B880•$^+$ spectral shapes are initially more Gaussian and progressively acquire increased Lorentzian character as $\chi$ increases.

These results may be consistent with a spin-exchange induced narrowing of the B880•$^+$ spectrum arising from the production of multiple radical cations within the B880 complex. The radical cations are distributed such that some complexes contain one B880•$^+$, whereas others contain two or more B880•$^+$ species. The complexes with $N$ sites containing $x$ spins occur with a probability $P_xN$. If it is assumed that the pigments are oxidized at random, then $P_xN$ can be calculated from the binomial distribution function $[N!/(N - x)!x!]\chi^x(1 - \chi)^{N-x}$. Using $\chi = 0.002$ as an example of a mildly oxidized sample and $N = 32$, then about 6% of the LH1 complexes contain one unpaired spin and roughly 0.2% of the complexes contain two spins; rings with a greater number of spins occur with negligible probability. The fraction of LHCs with multiple cations increases with increasing $\chi$. In B880 rings containing multiple spins, orbital interactions between proximally located B880•$^+$ species induce a mutual exchange of spin states. It is reasonable to surmise that intraring processes dominate interring contributions, since orbital exchange interactions decrease in a roughly exponential manner with increasing distance.

The spin-exchange process can proceed via one of two pathways. In the first pathway, spin exchange occurs within arrays of pigments containing multiple unpaired spins and in the absence of electron transfer. Orbital interactions within such arrays induce fluctuations of the spin states. These fluctuations produce pseudorandom changes of the electron spin resonance frequency (or correspondingly the magnetic field) such that the EPR spectrum is narrowed and becomes non-Gaussian with increasing $\chi$. The width decreases and the line shape changes with an increase of $\chi$ because the number of spins in close proximities is increased in the LH1 samples that are more oxidized. The low values of $\chi$ and the short-range interactions of spin exchange do not favor this mechanism. Alternatively, spin exchange can proceed via the collisions of unpaired electron spins that are mediated by electron transfer within the B880 rings. In this case, the spin-exchange rate increases with an increasing number of unpaired electrons in the rings. Such a process is analogous to bimolecular spin exchange reactions in solution where the rate increases with increasing concentrations of participating molecules.[43] Accordingly, the spectrum due to rings with *more* spins is probably narrower than that of rings with *fewer* spins. The contributions of the narrower spectra increase with $\chi$, since the radical cation distribution shifts toward rings with a greater number of B880•$^+$ (see above). The observed spectrum, which is the probability-weighted sum of the spectra of rings with $x$ spins each, is thus progressively narrowed with increased oxidation of LH1. According to this pathway, the line narrowing occurs due to random frequency (field) fluctuations engendered by both electron transfer and electron-transfer-mediated spin exchange. The results of variable temperature EPR measurements, which are reported in the following section, strongly support this line narrowing mechanism.

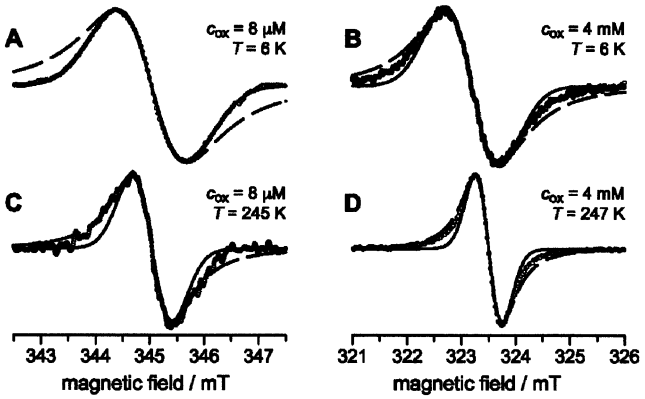


**Figure 4.** Temperature dependence of detergent-isolated B880•$^+$ EPR spectra. The solid and dashed lines represent Gaussian and Lorentzian curves calculated with the widths of the experimental spectra (symbols). Spectra A and C were acquired for radical cations elicited with an 8 $\mu$M final concentration of PF. The 6 K spectrum is characterized by a Gaussian shape and a width of about 1.3 mT, whereas the 245 K spectrum exhibits a non-Gaussian shape and a narrowed 0.73 mT width. Spectra B and D were measured for a sample oxidized with a 4 mM final concentration of PF. The 6 and 247 K spectra both exhibit non-Gaussian line shapes. The spectral width decreases with an increase in temperature from about 1.07 mT at 6 K to 0.49 mT at 247 K.

In concluding this section we note, that the width and shape may also be somewhat affected by exchange broadening due to interactions between B880•$^+$ and $Fe^{3+}$ and/or $Fe^{2+}$. This effect is expected to be more marked for detergent-isolated B880•$^+$, since the detergent micelles are less effective at shielding the LH1 BChl*a*s. That this is the case is indicated by the facile manner in which the detergent-isolated complexes are oxidized compared to membrane-bound LH1 (see above).

**B. Variation of the B880•$^+$ EPR Spectral Parameters with Temperature.** The UV/visible spectra of oxidized LH1 samples were acquired at room temperature. EPR spectra were measured in the temperature range from 80 to 300 K for detergent-isolated LH1 samples that showed $\chi$ values of 0.002, 0.009, and 0.157. These samples were generated with 7 $\mu$M, 0.1 mM, and 4 mM final concentrations of PF. Additionally, EPR spectra in the 6−300 K temperature range were measured for detergent-isolated B880•$^+$ samples that were generated with 8 $\mu$M and 4 mM final concentrations of PF.

Variable temperature measurements were also conducted on oxidized membrane bound LH1. The overall behavior detected for these samples was analogous to that observed for detergent-isolated complexes such that the results are not reported here. We note that control measurements were performed on samples oxidized with ammonium cerium nitrate. The results were highly similar to those obtained for LH1 treated with PF, which demonstrates that the nature of the oxidant is unimportant in determining the EPR characteristics of B880•$^+$.

*B.1. Basic EPR Unit of the B880 LH1 Complex.* Parts A and B of Figure 4 display B880•$^+$ EPR spectra acquired at a temperature of 6 K. These are compared to Gaussian and Lorentzian curves calculated with the widths of the experimental spectra. The radical cations were generated with PF concentra-

tions ($c_{ox}$) of 8 $\mu$M and 4 mM, respectively. The spectrum of B880$\bullet^+$ ($c_{ox}$ = 8 $\mu$M) is well-described by a Gaussian curve with a line width of 1.29 mT. Such characteristics were detected for B880$\bullet^+$ *only* under these conditions of oxidation and temperature. B880$\bullet^+$ generated with a 4 mM oxidant concentration exhibits a significantly non-Gaussian spectrum with a narrower width of about 1.07 mT. The shape and width reductions are due to spin exchange, which occurs because of the increased number of spins in the B880 rings. It is evident that the spectrum elicited with the lower PF concentration to a good approximation represents a magnetically dilute system.

At 6 K, monomeric BChl*a*$\bullet^+$ in methanol/glycerol glass exhibits a Gaussian spectrum with a width of about 1.4 mT.[44] (The width is increased relative to the 1.35 mT value detected at temperatures greater than 80 K due to the frozen rotation of methyl groups located on rings I and III of the macrocycle.) The similarity of the 6 K B880$\bullet^+$ ($c_{ox}$ = 8 $\mu$M) spectral characteristics to that measured for monomeric BChl*a*$\bullet^+$ suggests that the basic EPR unit of B880$\bullet^+$ is a BChl*a* monomer or a highly asymmetrical dimer. According to this view, the slight reduction in EPR line width for B880$\bullet^+$ occurs because of slow spin migration between monomeric B880 units. Simulations, which are detailed in section B.3, show that spin migration proceeding at a rate of about $2.3 \times 10^6$ s$^{-1}$ to $4.2 \times 10^6$ s$^{-1}$ would reduce the width from 1.35 mT or 1.4 mT to 1.29 mT without causing significant deviation from a Gaussian line shape. That the basic unit of B880$\bullet^+$ from the EPR point of view is monomeric BChl*a*$\bullet^+$ is also indicated by the results of EPR measurements conducted on oxidized B820 complexes.[45] These pigment−protein assemblies are a subunit form of LH1 with a $\alpha\beta$(BChl*a*)$_2$ structure. In the 80−240 K temperature range, B820$\bullet^+$ exhibits a Gaussian EPR spectrum with a 1.33 mT width. These characteristics closely correspond to those detected for monomeric BChl*a*$\bullet^+$.

An alternative interpretation of the 6 K B880$\bullet^+$ ($c_{ox}$ = 8 $\mu$M) spectrum is that it is due to spins that are delocalized over a pair of dissimilar BChl*a*s. It is well-established that an asymmetric distribution of the spin over two halves of a dimer will engender a monomer-like EPR spectrum.[32] This phenomenon is exemplified by the BChl*b*s comprising the primary electron donor (P960) of *Rps. viridis*, where the radical cation P960$\bullet^+$ exhibits a monomer-like width of 1.18 mT instead of the 0.95 mT width expected for a symmetric dimer.[39] The spin-density distribution in the primary electron donor radical cation of RCs is in general found to be unequal over the two halves of the dimer due to deviations from perfect $C_2$ symmetry. The disruption of symmetry is attributed to perturbations of the BChl*a* structure and to the different protein environments near the two halves of the super molecular dimer.[46−50] Such conditions most certainly obtain for the LH1 BChl*a*s, which are bound to homologous but not identical $\alpha$- and $\beta$-peptides. Additionally, Raman spectroscopy of LH1 complexes has indicated that the BChl*a*s in the B880 complex are distorted.[51,52] These factors can contribute to an asymmetric distribution of spin densities over a dimer of BChl*a*s. In this interpretation the fundamental EPR unit is a highly asymmetrical dimer.

*B.2. Electron Transfer in the B880 Complex.* Parts C and D of Figure 4 display B880$\bullet^+$ ($c_{ox}$ = 8 $\mu$M and 4 mM) spectra measured at a temperature of about 245 K. These are compared to Gaussian and Lorentzian curves calculated with the widths of the experimental spectra. The spectra are non-Gaussian with widths that are significantly reduced relative to the 6 K values; see Figure 4A,B. The shapes and decreased line widths are due to motional narrowing. In the case of B880$\bullet^+$ ($c_{ox}$ = 8 $\mu$M), which is a magnetically dilute system, the line narrowing must be due to thermally activated electron transfer. In other work, we have demonstrated that such a process narrows the BChl*a* radical cation spectrum in B820 subunits of LH1 complexes.[45] Thermally activated electron transfer was also shown to narrow the chlorophyll (Chl) radical cation EPR spectrum in oxidized Chl micelles.[53] The B880$\bullet^+$ ($c_{ox}$ = 4 mM) spectrum at 247 K exhibits a line width of about 0.49 mT, which is smaller than the 0.73 mT width detected for B880$\bullet^+$ elicited with the 8 $\mu$M oxidant concentration. In this case the width reduction occurs due to both electron transfer and spin exchange. The exchange process most likely occurs via collisions between itinerant spins. Such a process was shown to narrow the EPR spectra of synthetic porphyrin oligomers.[54−58]

Parts A and B of Figure 5 display the temperature dependence of B880$\bullet^+$ EPR line widths for samples that were oxidized to different extents. The line widths decrease significantly with increasing temperature. In the case of B880$\bullet^+$ ($\chi$ = 0.002), which was generated with a 7 $\mu$M final concentration of oxidant, and B880$\bullet^+$ ($c_{ox}$ = 8 $\mu$M), the width variations occur mainly due to electron transfer. Under the mild oxidation conditions, rings with a greater number of spins occur with negligible probabilities. This result additionally supports the assignment of the line width changes to electron transport. Samples treated with larger oxidant concentrations exhibit narrower line widths. This is due to increased contributions from electron-transfer-mediated spin exchange.

Another reason for such a dependence on the oxidant concentration may be an inhomogeneous distribution of the oxidation potentials of BChl*a*s. In such an explanation, BChl*a*s with low oxidation potentials may behave as traps for the holes. When the number of oxidized holes is small, all may be trapped and immobile. With increasing concentration of oxidant, more untrapped holes appear and speed up the overall rate of the electron transfer.

Dynamical processes such as electron transport and spin exchange are expected to engender rate dependent spectral widths and shapes. The B880$\bullet^+$ spectra were fit with the Voigt profile in order to verify that the line shapes did in fact change with temperature. The results for B880$\bullet^+$ ($\chi$ = 0.157) are shown in Figure 5

C. The line shape descriptors $\Delta H_G$ and $\Delta H_L$ vary with temperature, which reflects changes of the B880$\bullet^+$ EPR spectral shape. Such variations of the shape with temperature were detected for all of the investigated samples.

We note that both monomeric BChl*a*$\bullet^+$ and P865$\bullet^+$ exhibit width decreases of about 0.05 mT in the 2−80 K temperatures range.[44] Simultaneous significant changes of the line shapes are not detected; that is, the spectra retain Gaussian shapes. At about 2 K, the methyl group rotations are frozen. The protons show individual couplings to the electron spin, resulting in an increased spectral width. The protons become equivalent due to rapid rotation at about 80 K, and the width reaches a limiting value. It is likely that such a process contributes in addition to spin motion to the changes of the B880$\bullet^+$ spectrum in the 6−80 K temperature range. The energetics of the rotation process, however, are expected to be different for B880$\bullet^+$ compared to either BChl*a*$\bullet^+$ or P865$\bullet^+$ due to differences in the environments surrounding the methyl groups. The B880$\bullet^+$ width increases very rapidly at temperatures less than about 10 K. This broadening occurs due to progressively decreasing rates of spin migration, probably with contributions accruing from freezing of methyl group rotations. The trend of the B880$\bullet^+$ data indicates

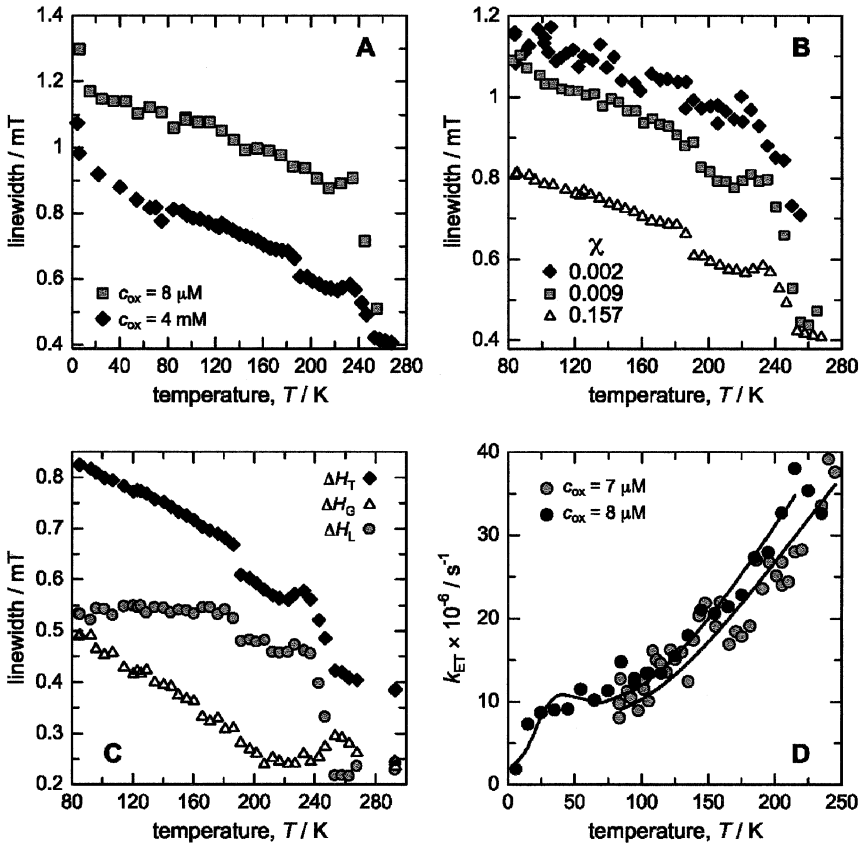


**Figure 5.** (A and B) Temperature dependence of detergent-isolated B880•$^+$ EPR line widths. The data are for (A) LH1 complexes that were oxidized with 8 $\mu$M and 4 mM final concentrations of PF and (B) samples that exhibited LH1 near-infrared bleaches of 0.2, 0.9, and 15.7%, respectively. These were generated with 7 $\mu$M, 0.1 mM and 4 mM final concentrations of PF. (C) Temperature dependence of detergent-isolated B880•$^+$ EPR line shape parameters, where $\Delta H_T$ is the envelope line width and $\Delta H_G$ and $\Delta H_L$ are the Gaussian and Lorentzian widths, respectively. These parameters were extracted from Voigt profile fits to the spectra. The LH1 sample used for this measurement exhibited a 15.7% bleach of the BChl*a* near-IR band. (D) Temperature dependence of charge transport rates, which were extracted from the B880•$^+$ EPR line width data. The solid lines represent fits to the rate versus temperature profiles calculated with the nonadiabatic electron-transfer model of Tang (see text for details).

that the monomeric BChl*a*•$^+$ width will be obtained at temperatures less than 6 K.

The B880•$^+$ line width versus temperature profiles exhibit abrupt changes at about 187 and 247 K. We attribute these features to glass transition induced changes of the spin migration rates.[59] In the case of electron transport, the rate variation can occur due to the temperature activation of quiescent medium modes. The changes of the electron-transfer rate would affect the spin exchange rate as well. Glass transitions may also cause changes of the structure of the B880 ring. This would alter the electronic couplings between the pigments, and hence, affect the rates of electron transfer and spin exchange. A mechanism involving variations of the pigment arrangements is supported by the observation of glass transition driven structural changes of the B850 ring in LH2 complexes.[60−62] The B880•$^+$ data also display a broader width variation with a maximum at approximately 233 K. A similar feature centered at about 250 K is detected in the temperature dependence of P865•$^+$ line widths.[63] This observation suggests that the variation in line width is unrelated to spin migration and is instead produced by changes of the electron-spin relaxation rates.

*B.3. Analysis of Cryogenic Electron Transfer in B880•$^+$.* The EPR spectral shapes and widths of B880•$^+$ generated with 7 and 8 $\mu$M concentrations of PF exhibit significant changes with temperature (see Figure 5A,B). In the case of B880•$^+$ ($c_{ox}$ = 8 $\mu$M) for instance, the line width decreases from 1.29 mT at 6 K to about 0.51 mT at 255 K. A similar line width decrease is also detected for B880•$^+$ elicited with the 7 $\mu$M oxidant concentration. Under the mild oxidation conditions employed in eliciting the radical cations, only B880 rings with a single spin occur with significant probability. The observed temperature and width changes are mainly due to electron transport, which occurs even close to liquid helium temperatures.

The charge transport rates were extracted via comparison of simulated spectra to experimental data. The calculations incorporated electron−nuclear hyperfine interactions as the sole line-broadening process. This is consistent with the Gaussian shape of the B880•$^+$ ($c_{ox}$ = 8 $\mu$M) 6 K spectrum, which indicates negligible electron−spin dipolar and exchange interactions. Additionally, it is well-established that other broadening processes such as **g**-anisotropy contribute only minimally to BChl*a*•$^+$ spectra at X-band frequencies.[39] The basic EPR unit of the B880 complex was taken as monomeric BChl*a*•$^+$, which is in accordance with the characteristics of the 6 K spectrum. The monomer spectrum contains transitions due to molecules with different nuclear spin configurations. For organic radicals in general, and dilute BChl*a*•$^+$ species in particular, the various spin relaxation times are quite long ($T_1$, $T_2$ > 1 $\mu$s). That this is the case for monomeric BChl*a*•$^+$ is directly indicated by the Gaussian line shape, where the spectrum represents a "static" inhomogeneous distribution. The B880s can thus be considered as groups of $N$ molecules chosen at random from the monomer distribution. The nuclear spin configurations at the $N$ sites occur in a mutually independent manner. For this reason the probabilities of obtaining the various $N$-mers is $P(\omega_1, \omega_2, ..., \omega_N) = P(\omega_1)P(\omega_2)...P(\omega_N)$, where the $\omega_i$ are the resonance frequencies

of the spins at the $N$ sites. For a normalized EPR spectrum $P(\omega_i)$ are the intensities at $\omega_i$. The $N$-mers occurring with probabilities, $P(\omega_i)$, comprise subensembles. The observed spectrum is the probability-weighted sum of the spectra of all subensembles. The subensemble spectra were calculated using the model of Anderson[64] and Kubo.[65] In this model, the autocorrelation function of the magnetic moment, $S(t)$, which incorporates the effect of frequency fluctuations, is calculated first. The line shape function, $I(\omega)$, is then obtained as the Fourier transform of $S(t)$. The calculation of $S(t)$, $S(t) = \langle M^*(0)\ M(t)\rangle\ /\langle M^*(0)\ M(0)\rangle$, where $M$ is the magnetic moment of the system, involves solving the equation of motion for $M(t)$. For this purpose, the precession frequency, $\omega(t)$, is considered as a stochastic variable that adopts the values $\omega_i$ as the spins jump randomly between $N$ sites. By modeling the random changes of $\omega(t)$ as a Markovian process, and, neglecting saturation effects, the stochastic equation for $M(t)$ is solved to yield

$$S(t) = \boldsymbol{\varphi} e^{[(i\boldsymbol{\Omega}+\mathbf{W})t]}\phi, \quad t > 0$$

$$S(-t) = S^*(t) \tag{1}$$

where $\boldsymbol{\varphi}$ is a vector with elements $(\varphi_i)$ proportional to the occupational probabilities of the $N$ sites at equilibrium, $\phi$ is a vector with $N$ elements equal to unity, $\boldsymbol{\Omega}$ is a $N \times N$ diagonal matrix with elements $(\omega_i)$ equal to the resonance frequency of the spin at the various sites. The $N \times N$ matrix $\mathbf{W}$ contains off-diagonal elements equal to $w_{jk}$, which are the rate constants for spin migration from the $k$th to the $j$th site, and diagonal elements equal to where $T_2$ is the electron spin transverse

$$-T_2^{-1} - \sum_{j=1}^{N} w_{jk}, \quad j \neq k, \tag{2}$$

relaxation time. Equation 1 can be readily computed by diagonalizing the matrices $i\boldsymbol{\Omega} + \mathbf{W}$, in which case $S(t)$ is expressed as a sum of exponentials. The line shape function, $I(\omega)$, is the real part of the Fourier transform of $S(t)$. This is a sum of resonance distributions, which in terms of the coefficients, $c_i$, and the eigenvalues, $\lambda_i$, is represented as

$$I(\omega) \propto -\sum_{i=1}^{N} \frac{\mathrm{Re}(c_i)\ \mathrm{Re}(\lambda_i) + \mathrm{Im}(c_i)[\mathrm{Im}(\lambda_i) - \omega]}{\mathrm{Re}(\lambda_i)^2 + [\mathrm{Im}(\lambda_i) - \omega]^2} \tag{3}$$

$$c_i = \sum_{j=1}^{N} \varphi_j u_{ji} \sum_{k=1}^{N} v_{ik}$$

where Re( ) and Im( ) denote the real and imaginary components of the complex numbers and, $u_{ji}$ and $v_{ik}$ are elements of the matrix of eigenvectors and its inverse, respectively.

The charge transport process in the B880 complex was taken to proceed via a nearest-neighbor mechanism along a closed loop containing $N = 32$ pigments. This model was suggested by the following considerations. Structural data for LH1 indicate that 32 B880s are arranged as an overlapping circular array sandwiched between two concentric rings formed by the α- and $\beta$-peptides. The BChl*a*s within a B880 complex exhibit Mg−Mg separations of about 0.9 nm, whereas the shortest distance between macrocycles located on neighboring LH1 complexes is about 2.2 nm.[66] Given that the electron-transfer rate decreases with increase of distance as $w \propto \exp(-\beta R)$, where $\beta$ is an attenuation coefficient with a value of about 10 $\mathrm{nm}^{-1}$ and $R$ is the separation, it is calculated that interring electron transport will occur with a rate that is about 6 orders of magnitude smaller than the rate of intraring transport. Similar considerations apply to intraring charge transport, for which, assuming a separation of 1.8 nm between once removed BChl*a*s, it is calculated that the rate is about 4 orders of magnitude smaller than that between nearest neighbors.

An additional simplification was introduced in the model with the assumption of identical rates between all $N$ sites. This corresponds to isoenergetic charge transport that proceeds between equally coupled pigments. The rationale for this simplification is that since the LH1 BChl*a*s are all present in similar protein environments, the free energy gaps for interpigment charge transport to a good approximation must be identical and equal to zero. Further, results of ab initio calculations for LH2 indicate similar electronic couplings between all BChl*a*s in the B850 ring,[11] which suggests that the same must be obtained for the B880 complex of LH1. In this study, the effect of slow and medium relaxation processes on charge transport is neglected. That such processes affect the charge transport rates is indicated by the abrupt glass transition induced changes of the line widths at 187 and 247 K. It must also be noted that the optical absorption spectra of antenna complexes are inhomogeneously broadened due to energetic disorder.[29] It is possible that the optical disorder is connected to the medium relaxation phenomena detected in the EPR temperature dependence. In this analysis, we restricted ourselves to the simplest and possibly the most descriptive charge transport model with the expectation that deviations from the ideal would reveal the contributions of energetic disorder. With the above-elucidated set of assumptions regarding charge transport in the B880 ring, the transition matrix, $\mathbf{W}$, assumes a cyclic tridiagonal form with all nonzero off-diagonal elements equal to the charge transport rate ($w$) and all diagonal elements equal to $-T_2^{-1} - 2w$. Additionally, the elements of the vector $\boldsymbol{\varphi}$, which are the equilibrium occupational probabilities of the sites, become equal to $1/N$.

The spectral simulations were conducted in the field domain as follows. The diagonal elements of Ω were sampled from a Gaussian random number generator. The variance of the distribution was set at 0.675 mT, which corresponds to the 1.35 mT peak-to-peak line width of monomeric BChl*a*•$^+$. The matrix $i\boldsymbol{\Omega} + \mathbf{W}$ was first numerically diagonalized to obtain a vector containing the eigenvalues and a matrix containing the corresponding eigenvectors, following which the inverse of the eigenvector matrix was computed. The resonance distributions were calculated from these quantities using eq 3 and then added. The procedure was iterated until the shape converged, which typically occurred when about $2 \times 10^5$ groups of $N$ fields were sampled. The ensemble averaged spectra showed some "noise" due to the finite field intervals at which the intensities were calculated and due to the finite number of sampled hyperfine fields. The "noise" was particularly pronounced in the derivative. For this reason, the absorption mode spectra were smoothed before computing the derivative. Figure 6 illustrates some features of motionally narrowed spectra for closed loop $N$-mers.

The interpigment charge transport rates were extracted by obtaining a good visual fit between calculated and experimental spectra. A monomer width of 1.35 mT was utilized for the spectral simulations at all temperatures. The effect of methyl group rotations, if any, was neglected. This was because the energetics of the process is not determined in the present study, and more importantly, because using widths between 1.4 and 1.35 mT do not significantly alter the extracted charge-transport rates. The number of sites, $N$, was fixed at 32 for all simulations,

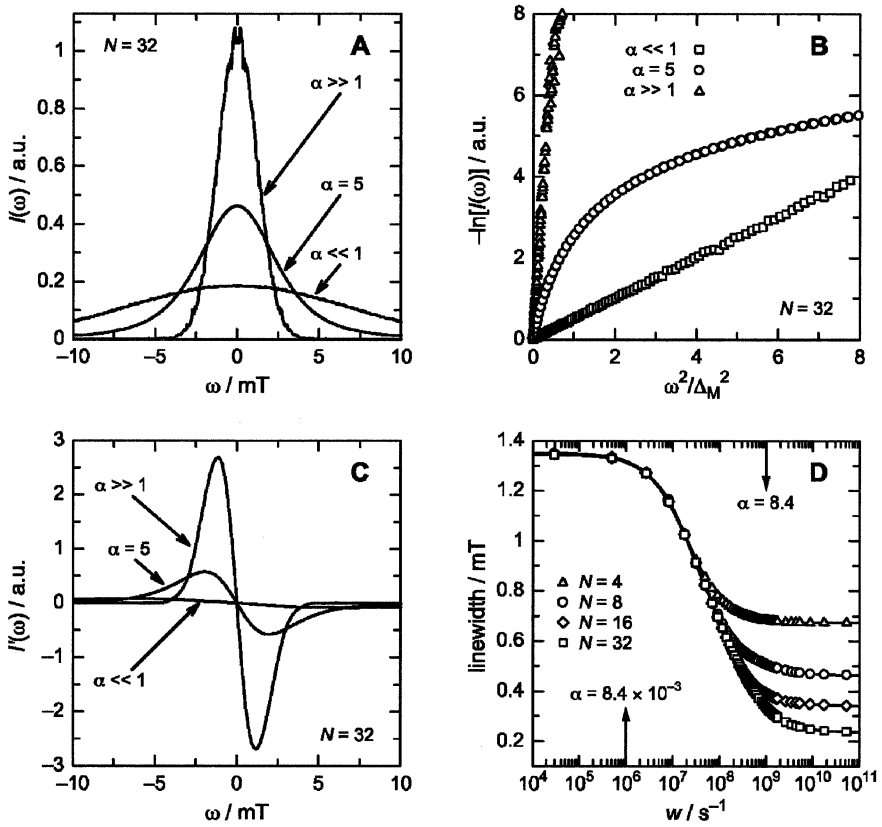


**Figure 6.** Characteristics of simulated EPR spectra for closed loop *N*-mers. The spin migration rates between the various sites were set to be equal to each other. The situation thus corresponds to isoenergetic electron transfer that proceeds between equally coupled molecules. The parameter α is defined as the ratio of the spin migration rate ($w$) to the variance of the monomer spectrum ($\Delta_M$) where $\alpha \ll 1$ and $\alpha \gg 1$ correspond to the slow and fast motion limits, respectively. Panel A shows EPR absorption spectra calculated for different regimes of motion. Panel B displays graphs of $-\ln[I(w)]$ versus $\omega^2/\Delta_M 2$. In this form, a Gaussian function will exhibit a linear dependence. In the slow and fast motion regimes, a linear variation is observed demonstrating that the spectra are Gaussian. The $\alpha = 5$ spectrum clearly deviates from a Gaussian line shape. Such line shapes are characteristic of the intermediate regime of motion. Panel C shows first derivative curves computed from smoothed absorption mode spectra. The peak-to-peak line widths were obtained as the difference of the field loci of the extrema. Panel D illustrates the variation of the peak-to-peak line width with the rate of spin migration. The width is extremely sensitive to the spin migration rate when the rate is within the $10^6$−$10^9$ $s^{-1}$ range. As the rate increases beyond $10^9$ $s^{-1}$, the width slowly approaches limiting values. The fast-motion-limit line widths in all cases were smaller than the 1.35 mT monomer width by factors of $N^{1/2}$. This is in agreement with the prediction of the delocalization or fast motion limit model.[30,40]

as is consistent with available structural data. Figure 7 compares simulated and experimental spectra at a few temperatures, where reasonable agreement between the calculated and experimental data is discerned. Similar results were obtained in the entire investigated temperature range.

The temperature dependence of the rates in the 6−247 K temperature range was interpreted on the basis of Tang's model for nonadiabatic electron transfer in order to obtain the energetic and electronic factors governing the interpigment charge-transport process.[67] According to this model, the temperature dependence of the rate ($w$) of an isoenergetic electron process is given as

$$w = \frac{2\pi V^2}{\hbar\sqrt{2\pi\sum_j \gamma_j^2 \hbar^2 \omega_j^2 \mathrm{csch}(\hbar\omega_j/2k_BT)}} \exp\left(-\sum_j \gamma_j^2 \tanh(\hbar\omega_j/4k_BT)\right) \quad (4)$$

$$\lambda \approx \sum_j \gamma_j^2 \hbar\omega_j,$$

where $V$ is the electronic coupling between the donor and acceptor states, $\omega_j$ are the frequencies of the vibration modes that are coupled with strengths $\gamma_j$ to the electron-transfer process, and $\lambda$ is the reorganization energy. Figure 5D displays fits to the charge-transport rates with eq 4. The parameters used were the matrix element, two vibration modes, and the associated coupling strengths. Rates extracted from spectra of samples oxidized with 7 and 8 $\mu$M concentrations of PF, respectively, yielded only marginally different values for the fit parameters. In both cases, a matrix element of about 0.8 $cm^{-1}$ and modes of about 28 and 352 $cm^{-1}$ with coupling strengths of 2.1 yielded satisfactory descriptions of the data. The reorganization energy of 1759 $cm^{-1}$ is calculated from the vibration mode parameters.

The values of the matrix elements obtained for both B880 and B820 are rather small. This is somewhat surprising given that the BChl*a*s in the B880 complex were anticipated to be essentially in van der Waals contact. As to why the pigments in the B880 complex exhibit such weak ground-state interactions while those in P865 couple strongly given the similar separations is an issue that merits investigation, but if LH2 is an appropriate model for LH1, then the BChl*a*s of LH1 are further apart than in the "special pair" primary donor.

The large value of $\lambda$ for B880 of this paper differs with the small value of $\lambda$ for B820 previously obtained from the analysis of the temperature dependence of the B820$^{\bullet+}$ EPR spectrum.[45] That work included complications of sample heterogeneity by treating the effects of glass transitions in the medium using the electron-transfer model of Hoffman and Ratner.[68] The treatment of Hoffman and Ratner can simulate steep variations of the

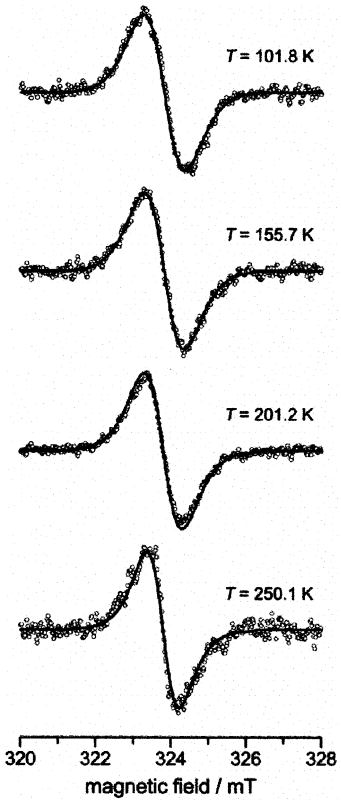


**Figure 7.** Comparison of simulated line shapes (lines) to experimental B880•$^+$ EPR spectra (symbols). The displayed experimental spectra are for the LH1 complexes that were oxidized with a 7 $\mu$M final concentration of PF. The charge transport rates used for the simulations were as follows: $k_{ET} \sim 1.1 \times 10^7$ s$^{-1}$ at 101.8 K, $k_{ET} \sim 1.4 \times 10^7$ s$^{-1}$ at 155.7 K, $k_{ET} \sim 1.9 \times 10^7$ s$^{-1}$ at 201.2 K, and $k_{ET} \sim 3.8 \times 10^7$ s$^{-1}$ at 250.1 K.

electron-transfer rate with decreasing temperature with reasonable values of the reorganization energy rather than the unrealistic values needed otherwise. In the case of the more simple dimeric B820 protein, physically plausible values of 125 cm$^{-1}$ for the reorganization energy and 0.25 cm$^{-1}$ for the matrix element were obtained.[45] Such low values of $\lambda$ are sensible because the reactions occur in frozen media where solvent/medium motion is severely restricted.

As discussed in section III.B, the heterogeneous distribution of oxidation potentials of B880 is likely the other factor, reducing the overall electron-transfer rate. This heterogeneous distribution would result in local differences in $\Delta G$ for the electron transfer between neighboring BChl*a*s even though the ensemble average of $\Delta G$ is zero. In the homogeneous electron-transfer model for B880 used in this paper, all values of $\Delta G$ are equal to zero. This forces the choice of a large value of $\lambda$ for B880 when fitting the strong temperature dependence of the electron-transfer rate. In the heterogeneous case of nonzero values of $\Delta G$, a strong dependence on temperature may be obtained while using smaller $\lambda$ values.

The option to address the heterogeneity issue of B880 as was done in B820 using a glass medium treatment is not applicable to the entire LH1 complex. In dealing with B820, a dimeric building block of the B880 of LH1, no significant possibility of multiple oxidation of a single dimer existed because of the low oligomer size of two combined with a low fraction of oxidation. Consequently, the temperature dependence of electron transfer in B820 involved only a single data set, easily treated within the framework of the model of Hoffman and Ratner. However, in B880, a different temperature dependence exists for each value of $\chi$. Since the Hoffman and Ratner model does not consider such complications, a more detailed model that considers redox heterogeneity explicitly is desirable. We thus conclude that only by explicitly treating redox heterogeneity in the modeling of cation migration in B880•$^+$ of LH1 will reasonable parameters of electron transfer be extracted. A detailed treatment of redox heterogeneity is left to future work.

**Acknowledgment.** We gratefully acknowledge C. N. Hunter (University of Sheffield) for *Rb. sphaeroides* strain M2192. In addition, support from the U. S. Department of Energy, Office of Basic Energy Sciences, Division of Chemical Sciences Contract DE-FG02-96ER14675 is gratefully acknowledged. S.W. thanks the Alexander von Humboldt Foundation (Bonn, Germany) for the award of a Feodor-Lynen fellowship. Experiments performed in Berlin have been supported by the Deutsche Forschungsgemeinschaft (DFG), Sonderforschungsbereich 498 (Teilprojekt A2).

## References and Notes

(1) Fleming, G. R.; van Grondelle, R. *Curr. Opin. Struct. Biol.* **1997**, *7*, 738.
(2) McDermott, G.; Prince, S. M.; Freer, A. A.; Hawthornthwaite-Lawless, A. M.; Papiz, M. Z.; Cogdell, R. J.; Isaacs, N. W. *Nature* **1995**, *374*, 517.
(3) Koepke, J.; Hu, X.; Muenke, C.; Schulten, K.; Michel, H. *Structure* **1996**, *4*, 581.
(4) Deisenhofer, J.; Epp, O.; Miki, K.; Huber, R.; Michel, H. *Nature* **1985**, *318*, 618.
(5) Allen, J. P.; Feher, G.; Yeates, T. O.; Komiya, H.; Rees, D. C. *Proc. Natl. Acad. Sci. U.S.A.* **1987**, *84*, 5730.
(6) Chang, C.-H.; Tiede, D.; Tang, J.; Smith, U.; Norris, J. R.; Schiffer, M. *FEBS Lett.* **1986**, *205*, 82.
(7) Karrasch, S.; Bullough, P. A.; Ghosh, R. *EMBO J.* **1995**, *14*, 631.
(8) Monshouwer, R.; van Grondelle, R. *Biochim. Biophys. Acta* **1996**, *1275*, 70.
(9) Chachisvilis, M.; Kühn, O.; Pullerits, T.; Sundström, V. *J. Phys. Chem. B* **1997**, *101*, 7275.
(10) Sauer, K.; Cogdell, R. J.; Prince, S. M.; Freer, A. A.; Isaacs, N. W.; Scheer, H. *Photochem. Photobiol.* **1996**, *64*, 564.
(11) Scholes, G. D.; Gould, I. R.; Cogdell, R. J.; Fleming, G. R. *J. Phys. Chem. B* **1999**, *103*, 2543.
(12) Rosenbachbelkin, V.; Fisher, J. R. E.; Scherz, A. *J. Am. Chem. Soc.* **1991**, *113*, 676.
(13) Koolhaas, M. H. C.; Frese, R. N.; Fowler, G. J. S.; Bibby, T. S.; Georgakopoulou, S.; van der Zwan, G.; Hunter, C. N.; van Grondelle, R. *Biochemistry* **1998**, *37*, 4693.
(14) Beekman, L. M. P.; Frese, R. N.; Fowler, G. J. S.; Picorel, R.; Cogdell, R. J.; van Stokkum, I. H. M.; Hunter, C. N.; van Grondelle, R. *J. Phys. Chem. B* **1997**, *101*, 7293.
(15) Jimenez, R.; Dikshit, S. N.; Bradforth, S. E.; Fleming, G. R. *J. Phys. Chem.* **1996**, *100*, 6825.
(16) Middendorf, T. R.; Mazzola, L. T.; Lao, K.; Steffen, M. A.; Boxer, S. G. *Biochim. Biophys. Acta* **1993**, *1143*, 223.
(17) Beekman, L. M. P.; Steffen, M.; van Stokkum, I. H. M.; Olsen, J. D.; Hunter, C. N.; Boxer, S. G.; van Grondelle, R. *J. Phys. Chem. B* **1997**, *101*, 7284.
(18) Warshel, A.; Parson, W. W. *J. Am. Chem. Soc.* **1987**, *109*, 6143.
(19) Fowler, G. J. S.; Visschers, R. W.; Grief, G. G.; van Grondelle, R. *Nature* **1992**, *355*, 848.
(20) Braun, P.; Scherz, A. *Biochemistry* **1991**, *30*, 5177.
(21) Engelhardt, H.; Engel, A.; Baumeister, W. *Proc. Natl. Acad. Sci. U.S.A.* **1986**, *83*, 8972.
(22) Ikeda-Yamasaki, I.; Odahara, T.; Mitsuoka, K.; Fujiyoshi, Y.; Murata, K. *FEBS Lett.* **1998**, *425*, 505.
(23) Miller, K. *Nature* **1982**, *300*, 53.
(24) Stahlberg, H.; Dubochet, J.; Vogel, H.; Ghosh, R. *J. Mol. Biol.* **1998**, *282*, 819.
(25) Stark, W.; Kühlbrandt, W.; Wildhaber, I.; Wehrli, E.; Mühlethaler, K. *EMBO J.* **1984**, *3*, 777.
(26) Walz, T.; Ghosh, R. *J. Mol. Biol.* **1997**, *265*, 107.
(27) Walz, T.; Jamieson, S. J.; Bowers, C. M.; Bullough, P. A.; Hunter, C. N. *J. Mol. Biol.* **1998**, *282*, 833.
(28) Jungas, C.; Ranck, J.; Rigaud, J.; Joliot, P.; Verméglio, A. *EMBO J.* **1999**, *18*, 534.
(29) Sundström, V.; Pullerits, T.; van Grondelle, R. *J. Phys. Chem. B* **1999**, *103*, 2327.

(30) Norris, J. R.; Uphaus, R. A.; Crespi, H. L.; Katz, J. J. *Proc. Natl. Acad. Sci. U.S.A.* **1971**, *68*, 625.
(31) Bowman, M. K.; Norris, J. R. *J. Am. Chem. Soc.* **1982**, *104*, 1512.
(32) Rautter, J.; Lendzian, F.; Lubitz, W.; Wang, S.; Allen, J. P. *Biochemistry* **1994**, *33*, 12077.
(33) Gomez, I.; Sieiro, C.; Ramirez, J. M.; Gomez-Amores, S.; del-Campo, F. F. *FEBS Lett.* **1982**, *144*, 117.
(34) Gomez, I.; Sanchez, A.; del-Campo, F. F. *Physiol. Veg.* **1985**, *23*, 583.
(35) Gingras, G.; Picorel, R. *Proc. Natl. Acad. Sci. U.S.A.* **1990**, *87*, 3405.
(36) Picorel, R.; Lefebvre, S.; Gingras, G. *Eur. J. Biochem.* **1984**, *142*, 305.
(37) Hunter, C. N.; Vangrondelle, R.; Vandorssen, R. J. *Biochim. Biophys. Acta* **1989**, *973*, 383.
(38) Smirnov, A. I.; Belford, R. L. *J. Magn. Reson. A* **1995**, *113*, 65.
(39) Lubitz, W. The Chlorophylls. In *BChla Coupling Constants*; Scheer, H., Ed.; CRC Press: Boca Raton, FL, 1991; p 903.
(40) Norris, J. R.; Katz, J. J. The Photosynthetic Bacteria. In *Oxidized Bacteriochlorophyll as Photoproduct*; Clayton, R. K., Sistrom, W. R., Eds.; Plenum Press: New York, 1978.
(41) Tang, J.; Dikshit, S. N.; Norris, J. R. *J. Chem. Phys.* **1995**, *103*, 2873.
(42) Law, C. L.; Cogdell, R. J. *FEBS Lett.* **1998**, *432*, 27.
(43) Molin, N. Y.; Salikhov, K. M.; Zamaraev, K. I. *Spin Exchange: Principles and Applications in Chemistry and Biology*; Springer-Verlag: Berlin, 1980.
(44) Feher, G.; Hoff, A. J.; Isaacson, R. A.; Ackerson, L. C. *Ann. N. Y. Acad. Sci.* **1975**, *244*, 239.
(45) Srivatsan, N.; Norris, J. R. *J. Phys. Chem. B* **2001**, *105*, 12391
(46) Plato, M.; Lendzian, F.; Lubitz, W.; Möbius, K. Molecular Orbital Study of Electronic Asymmetry in Primary Donors of Bacterial Reaction Centers. In *The Photosynthetic Bacterial Reaction Center II. Structure, Spectroscopy, and Dynamics*; Verméglio, J. B. A., Ed.; Plenum Press: New York, 1992; Vol. 237, p 109.
(47) Lubitz, W.; Rautter, J.; Käss, H.; Lendzian, F. *Sol. Energy Mater. Sol. Cells* **1995**, *38*, 77.
(48) Rautter, J.; Lendzian, F.; Schulz, C.; Fetsch, A.; Kuhn, M.; Lin, X.; Williams, J. C.; Allen, J. P.; Lubitz, W. *Biochemistry* **1995**, *34*, 8130.
(49) Allen, J. P.; Artz, K.; Lin, X.; Williams, J. C.; Ivancich, A.; Albouy, D.; Mattioli, T. A.; Fetsch, A.; Kuhn, M.; Lubitz, W. *Biochemistry* **1996**, *35*, 6612.
(50) Lendzian, F.; Rautte, J.; Käs, H.; Gardiner, A.; Lubitz, W. *Ber. Bunsen-Ges.* **1996**, *100*, 2036.
(51) Mattioli, T. A.; Hoffmann, A.; Sockalingum, D. G.; Schrader, B.; Robert, B.; Lutz, M. *Spectrochim. Acta, Part A* **1993**, *49*, 785.
(52) Chumanov, G.; Picorel, R.; de Zarate, I. O.; Cotton, T. M.; Seibert, M. *Photochem. Photobiol.* **2000**, *71*, 589.
(53) Bowman, M. K.; Michalski, T. J.; Tyson, R. L.; Worcester, D. L.; Katz, J. J. *Proc. Natl. Acad. Sci. U.S.A.* **1988**, *85*, 1498.
(54) Seth, J.; Palaniappan, V.; Johnson, T. E.; Prathapan, S.; Lindsey, J. S.; Bocian, D. F. *J. Am. Chem. Soc.* **1994**, *116*, 10578.
(55) Seth, J.; Palaniappan, V.; Wagner, R. W.; Johnson, T. E.; Lindsey, J. S.; Bocian, D. F. *J. Am. Chem. Soc.* **1996**, *118*, 11194.
(56) Yang, S. I.; Seth, J.; Strachan, J. P.; Gentemann, S.; Kim, D.; Holten, D.; Lindsey, J. S.; Bocian, D. F. *J. Porphyrins Phthalocyanines* **1999**, *3*, 117.
(57) Li, J. Z.; Ambroise, A.; Yang, S. I.; Diers, J. R.; Seth, J.; Wack, C. R.; Bocian, D. F.; Holten, D.; Lindsey, J. S. *J. Am. Chem. Soc.* **1999**, *121*, 8927.
(58) Li, J. Z.; Diers, J. R.; Seth, J.; Yang, S. I.; Bocian, D. F.; Holten, D.; Lindsey, J. S. *J. Org. Chem.* **1999**, *64*, 9090.
(59) Dick, L. A.; Malfant, I.; Kuila, D.; Nebolsky, S.; Nocek, J. M.; Hoffman, B. M.; Ratner, M. A. *J. Am. Chem. Soc.* **1998**, *120*, 11401.
(60) Wu, H.-M.; Reddy, N. R. S.; Small, G. J. *J. Phys. Chem. B* **1997**, *101*, 651.
(61) Wu, H.-M.; Ratsep, M.; Jankowiak, R.; Cogdell, R. J.; Small, G. J. *J. Phys. Chem. B* **1997**, *101*, 7641.
(62) Wu, H., -M.; Ratsep, M.; Lee, I.-J.; Cogdell, R. J.; Small, G. J. *J. Phys. Chem. B* **1997**, *101*, 7654.
(63) Dikshit, S. N. Investigations of Purple Bacterial Light Harvesting Complexes Using Electron Paramagnetic Spectroscopy. Ph.D., University of Chicago, 1998.
(64) Anderson, P. W. *J. Phys. Soc. Jpn.* **1954**, *9*, 316.
(65) Kubo, R. *J. Phys. Soc. Jpn.* **1954**, *9*, 935.
(66) Hu, X.; Schulten, K. *Biophys. J.* **1998**, *75*, 683.
(67) Tang, J. *J. Chem. Phys.* **1993**, *99*, 5828.
(68) Hoffman, B. M.; Ratner, M. A. *Inorg. Chim. Acta* **1996**, *243*, 233.